Evaluation of Electromagnetic Shielding Effects on Wi-Fi CSI-Based Angle-of-Arrival Estimation Using a Human-Shaped Model

Kio Joko
Faculty of Science and Technology
Sophia University
Tokyo, Japan
k-joko-9g9@eagle.sophia.ac.jp

Masakatsu Ogawa
Faculty of Science and Technology
Sophia University
Tokyo, Japan
m-ogawa@sophia.ac.jp

Ohara Kazuya
Access Network Service
Laboratories
NTT, Inc.
Kanagawa, Japan
kazuya.ohara@ntt.com

***Abstract*— Passive indoor localization of device-free individuals is essential for applications like elderly care, intrusion detection, and smart homes. Current localization methods mainly fall into machine learning–based and analytical approaches. In this study, we focus on analytical methods. We introduce a dynamic Angle of Arrival (AoA) estimation technique using the Multiple Signal Classification (MUSIC) algorithm, incorporating filtering for Non-Line-of-Sight (NLOS) conditions by leveraging Wi-Fi Channel State Information (CSI). Two scenarios were compared to assess the impact of reflection on estimation accuracy: one with an Electromagnetic Shield (EMS) covering the target and another without shielding (No-EMS). EMS outperformed No-EMS in accuracy under Line-of-Sight (LOS) conditions, but both showed performance drops in NLOS scenarios, with EMS experiencing a greater decline. To mitigate degradation under NLOS conditions, a filtering method was proposed to detect NLOS segments from changes in AoA and decreases in the CSI amplitude of the static path. The detected segments were then corrected through linear interpolation. The median AoA error decreased by 14.3%, with average improvements of 15.8% under EMS and 11.1% under No-EMS, demonstrating that the proposed approach effectively suppresses outliers and improves dynamic AoA estimation in reflection-prone environments.**

Keywords— Wi-Fi CSI, Localization, Angle of Arrival

I. INTRODUCTION

Passive indoor localization of device-free individuals plays an important role in a wide range of applications such as elderly care, intrusion detection, and smart homes [1], [2]. In particular, elderly people often resist the continuous use of mobile devices or wearable sensors [3], while intruders may intentionally avoid carrying devices to evade detection. In these practical scenarios, realizing device-free localization is indispensable.

Early studies on indoor localization widely employed methods based on Received Signal Strength Indicator (RSSI) [4]. However, RSSI provides only power information over the entire channel, which imposes limitations on accuracy. Consequently, Channel State Information (CSI) has attracted increasing attention [5], [6]. CSI provides fine-grained information, including both amplitude and phase for each subcarrier, enabling applications such as high-accuracy localization and activity recognition [7], [8]. With the widespread use of Multiple Input Multiple Output (MIMO) in wireless LAN standards, CSI measurement with array antennas has become feasible, enabling approaches that exploit spatial resolution such as Angle-of-Arrival (AoA) estimation. Most conventional AoA-based studies assume that the target carries a device and utilize the direct path between transmitter and receiver [9]. In contrast, device-free localization relies on reflections from humans [10], and the key challenge is separating static reflections from walls and floors and dynamic reflections caused by human movement. Such dynamic reflections are typically much weaker than static multipath components, making robust AoA estimation particularly challenging in real environments.

When a moving object passes near the line-of-sight (LOS) path between the transmitter and receiver, the direct path—which should ideally remain a static component—can undergo noticeable temporal fluctuations. These fluctuations become mixed with human-induced dynamic reflections, making the separation between the two substantially more difficult. This loss of separability mainly occurs when the LOS component is disturbed by motion, leading to reduced AoA estimation accuracy.

Approaches to device-free localization can be broadly categorized into machine learning–based methods and analytical methods. A representative machine learning approach is fingerprinting [11], which requires extensive offline training and is vulnerable to environmental changes. In this study, we adopt an analytical approach based on AoA estimation that leverages dynamic reflection components contained in CSI.

Existing CSI-based analytical approaches, including Dynamic-MUSIC [10] and other AoA/ToF (Time of Flight) – enhanced models, mainly focus on device-free tracking using high-resolution path separation. These studies also report that AoA estimation degrades in diagonal receiver placements; however, they do not address how to suppress this degradation using AoA information alone. In addition, existing work does not consider differences in target material properties, and therefore does not examine how changes in reflection characteristics affect dynamic AoA estimation.

In this study, we experimentally evaluate dynamic AoA estimation using a moving human-shaped model both with and without electromagnetic shielding, and analyze how shielding modifies human-induced reflections and influences angle-estimation accuracy. Furthermore, to mitigate the estimation degradation caused by fluctuations of the static component during NLOS segments, we propose a NLOS-filtering approach that combines angular variation and CSI amplitude to identify and correct unreliable segments.

This study focuses on estimating the angle-of-arrival of a single device-free target using 5 GHz CSI measured with a 3×3 MIMO transceiver. The scope of this paper is limited to

dynamic AoA estimation and its error mitigation; position estimation or multi-person tracking is outside the scope. The objective of this study is to evaluate how the presence or absence of electromagnetic shielding on a moving human-shaped target affects dynamic AoA estimation, and to investigate methods for reducing angle estimation errors.

The remainder of this paper is organized as follows. Section II presents the AoA estimation method, Section III details the measurement environment, Section IV describes the filtering strategy, and Section V discusses the experimental results.

II. AoA Estimation Method

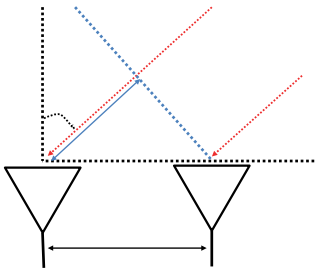

Fig.1 Antenna array with incidental signal.

Principle of AoA Estimation

AoA is estimated using the MUSIC algorithm. The estimation is made by utilizing the phase difference of the incoming signals at the antenna array. As illustrated in Fig. 1, if the antenna spacing is d, the incident angle is θ, and the wavelength is λ, then the path difference between adjacent antennas is $dsin\theta$, which corresponds to the phase delay

$$\Delta\varphi = \frac{2\pi dsin\theta}{\lambda}. \quad (1)$$

Based on this geometric relationship, the steering vector for an array with M antennas is expressed as

$$a(\theta) = [1, e^{-j\Delta\varphi}, e^{-j2\Delta\varphi}, \dots, e^{-j(M-1)\Delta\varphi}]^T. \quad (2)$$

At a given time instant t, CSI matrix is denoted by

$$H(t) \in \mathbb{C}^{T\times R\times S} \quad (3)$$

where T is the number of transmit antennas, R is the number of receive antennas and S is the number of subcarriers. Each column of $H(t)$ represents the channel response across the antenna array.

By performing eigenvalue decomposition of the covariance matrix, the signal and noise components can be separated. The covariance matrix C is defined as follows:

$$C = \frac{1}{N}\sum_{t=1}^{N} H(t)\cdot H(t)^H \quad (4)$$

where N is the number of samples. Applying eigenvalue decomposition to the covariance matrix C, we obtain

$$C = E\Lambda E^H. \quad (5)$$

The noise subspace E_n is extracted from E as the eigenvectors correspond to the smallest eigenvalues. Since the signal subspace is orthogonal to the noise subspace, the MUSIC spectrum is defined as

$$P_{MUSIC}(\theta) = \frac{1}{a(\theta)^H E_n E_n^H a(\theta)}. \quad (6)$$

and the angle that maximizes this spectrum is taken as the estimated AoA.

Extraction of Dynamic Components and CFO Removal

The raw received CSI contains strong static components such as the direct path from the signal source and reflections from walls and floors, and thus the dynamic reflections must be extracted. For each subcarrier S, let the time-series CSI be $H_s(t)$. Its temporal mean

$$\bar{H}_S = \frac{1}{t}\sum_{t=1}^{t} H_S(t) \quad (7)$$

is regarded as the static component $\bar{H}_S$, and the residual

$$\tilde{H}_S(t) = H_S(t) - \bar{H}_S \quad (8)$$

is used as the dynamic component $\tilde{H}_S(t)$ [10].

In addition, CSI contains time-varying phase rotations caused by Carrier Frequency Offset (CFO), which hinder the extraction of the dynamic components. To mitigate CFO, conventional studi es have proposed three schemes: dividing across transmit antennas (Tx-division) [12], dividing across receive antennas (Rx-division) [13], and conjugate multiplication between receive antennas (Rx-conjugate multiplication) [14]. Transmit-antenna division has been reported as the most effective [12]. CFO appears as a time-dependent complex phase rotation, and its effect can be mitigated by dividing CSI values measured at the same time or by applying complex conjugate multiplication. In transmit-antenna division, for two transmit antennas i and j, the relation is given by H_S^i/H_S^j.

To select appropriate transmit antennas and subcarriers for this division, the ratio between static and dynamic magnitudes is evaluated. For each transmit antenna and receive antenna pair, the mean magnitude of the static component and the maximum deviation magnitude of the dynamic component are computed for every subcarrier. The ratio of these magnitudes, averaged across receive antennas, indicates the dominance of the static path. The transmit antenna T^1 and subcarrier S^1 that yield the maximum ratio are used as the denominator, and the transmit antenna T^2 with the second-largest ratio is used as the numerator. Here, $h(p,T,R,S)$ is denotes the CSI of packet p : indexes packets within the analysis window. Consequently, the division

$$h(p,T^2,R,S^1) \,/\, h(p,T^1,R,S^1) \quad (9)$$

is applied. $h(p,T^1,R,S^1)$ is the static path and is used as the reference for the direct wave. After CFO removal, we apply a high-pass filter with a 1 Hz cutoff to capture moving-induced variations, and feed its CSI into the MUSIC algorithm for AoA estimation.

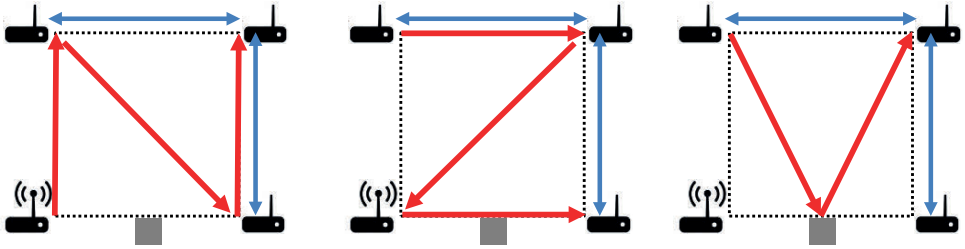

(a) Route “N” (b) Route “Z” (c) Route “V”

Fig. 2 Moving path of AMR for the measurement.

III. Measurement

The experiments were conducted in an indoor environment measuring 11.4 m × 10.2 m. A 4 m × 4 m measurement area was defined at the center of the room, where an autonomous mobile robot (AMR) carried a human-shaped polypropylene model. The AMR moved along three predefined trajectories (“N,” “Z,” and “V”) at a maximum speed of 1.0 m/s. Two target conditions were considered: (i) with electromagnetic shielding (EM-shielding) applied to the model, and (ii) without EM-shielding.

The EM-shielding consisted of a copper layer (1138 nm) and a nickel layer (268 nm), yielding a surface resistance of 0.02 Ω/square and a shielding effectiveness of 83 dB at 10 GHz. Although this material does not represent real human clothing, its high electrical conductivity systematically increases reflection strength. This design enables controlled evaluation of how reflection magnitude influences the separability of static and dynamic components in CSI. Materials with moderate conductivity—such as metallic-coated fabrics—can exhibit similar reflection enhancement, suggesting that the insights obtained here are relevant to practical indoor deployments.

Wi-Fi CSI was collected using the Linux 802.11n CSI Tool on the 5 GHz band with a 40 MHz channel bandwidth. The CSI sampling rate was 1000 Hz. Both the transmitter (Tx) and receivers (Rx0–Rx2) were equipped with three antennas, forming a 3×3 MIMO configuration with 2 cm antenna spacing. AoA estimation was later performed using a 1.0s window with a 0.1s shift. A LiDAR sensor recorded the ground-truth of the target, enabling accurate evaluation of visibility conditions and AoA estimation errors.

The spatial layout is shown in Fig. 2. The transmitter was placed at the lower-left corner of the measurement area, while the three receivers were positioned near the other corners: Rx0 (lower-right), Rx1 (upper-left), and Rx2 (upper-right). Due to this geometry, the extent of Non-Line-of-Sight (NLOS) exposure differs among the receivers. Based on LiDAR-based visibility analysis, Rx0 experiences NLOS segments primarily in the “Z” trajectory, Rx1 encounters NLOS segments in the “N” trajectory, and Rx2—located diagonally from the transmitter—encounters NLOS most frequently across all trajectories. Although the exact ratios depend on the path, Rx2 typically exhibits the longest cumulative NLOS duration. Each measurement sequence began with an empty environment for calibration, after which the AMR entered the measurement area and followed the designated trajectory.

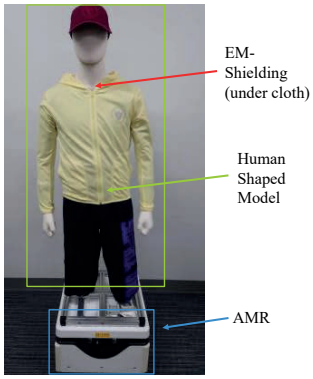

Fig.3 Human-shaped model and EM-Shielding.

IV. AoA Estimation Results

Figure 4 presents the AoA estimation accuracy for both the aggregated case (all routes combined) and each individual route. These results indicate that EM-shielding generally improves estimation accuracy compared with the No-EM-Shielding condition. However, for Rx2—which encounters NLOS regions across all trajectories—the estimation accuracy significantly degrades under both conditions, and this degradation becomes more pronounced when EM-shielding is applied. This behavior occurs because when the moving target passes near the LOS path and temporarily blocks it, the direct path— which should act as a time-invariant static component—begins to fluctuate over time. Once the static component becomes time-varying, the logic for separating static and dynamic reflections breaks down, and the MUSIC input covariance matrix no longer retains the structure needed for stable AoA estimation. Under EM-shielding, the LOS blockage to be more pronounced; as a result, the fluctuation of the static component becomes larger, leading to even greater degradation in NLOS segments.

Figure 5 shows the time-series AoA estimation results for the “N” route at Rx1 under both shielding conditions. The “N” route contains a NLOS segment between the transmitter and Rx1. Under the EM-shielding condition, the AoA estimation accuracy sharply deteriorates within the NLOS segment but remains high in the LOS segment. Under the No-EM-Shielding condition, the estimation error also increases in NLOS segments, although the overall estimation accuracy remains lower than in the shielded case.

Figure 6 plots the time variation in the CSI amplitude of the static path for the same route and receiver. The NLOS segments—identified from the LiDAR ground-truth trajectory—correspond to intervals where the CSI amplitude drops due to blockage of the direct path. This amplitude drop

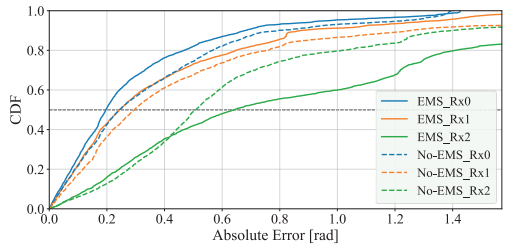

(a) CDF of AoA estimation results over all routes

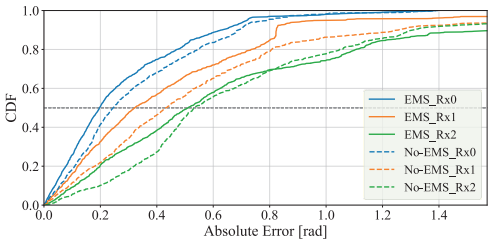

(b) CDF of AoA estimation results for "N" route

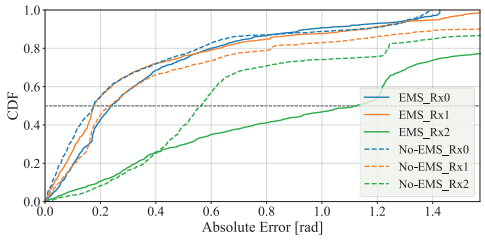

(c) CDF of AoA estimation results for "Z" route

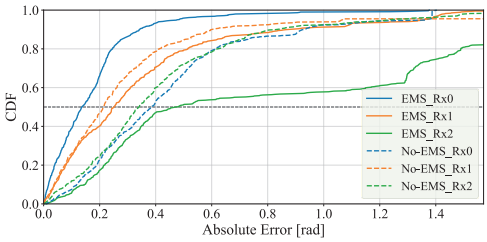

(d) CDF of AoA estimation results for "V" route

Fig. 4 CDF of AoA estimation results for each route..

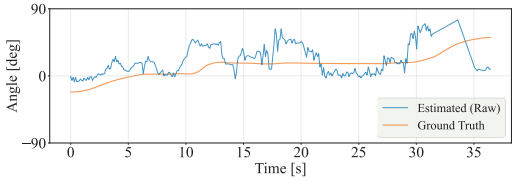

(a) EM-Shielding

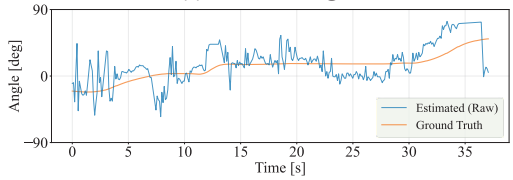

(b) No-EM-Shielding

Fig.5 AoA Estimation for route N, Rx1

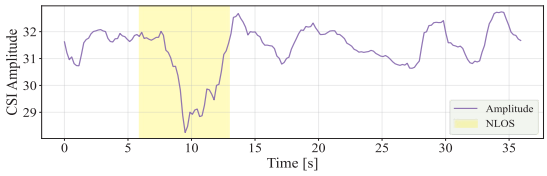

(a) EM-Shielding

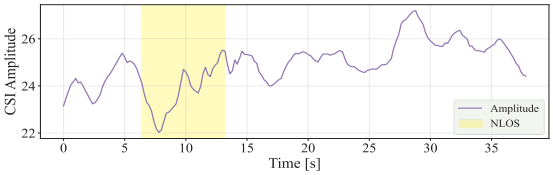

(b) No-EM-Shielding

Fig.6 CSI amplitude of the static path for route N, Rx1

is more evident under EM-shielding because the shielding material more effectively attenuates the direct path when the target blocks the LOS region, causing a sharper reduction in the static-path amplitude.

These observations indicate that large estimation errors often occur when the static component becomes unstable during NLOS transitions. Therefore, by detecting such segments using indicators such as abrupt changes in AoA estimates and decreases in static-path CSI amplitude, and by interpolating the corrupted intervals, the overall quality of dynamic AoA estimation would be improved.

V. Filtering Strategy

As observed in Section IV, large AoA estimation errors tend to occur when the static component becomes unstable during LOS–NLOS transitions. To mitigate these effects, we introduce a filtering strategy that detects unreliable intervals and corrects them through linear interpolation.

The proposed method identifies such intervals using a combined score derived from two indicators: the fluctuation of the estimated angle, and the attenuation of the static-path CSI amplitude. These indicators correspond to the two primary factors observed to cause estimation degradation.

Filtering Details

1. Scoring Angular Velocity

When the AMR approaches or leaves an NLOS region, the estimated AoA typically exhibits rapid and irregular variations due to fluctuations in the static component. To quantify this behavior, the angular velocity ω_n is obtained by differentiating the estimated angle:

$$\omega_n = \frac{d}{dt}\theta_n \tag{10}$$

The short-term variability of ω_n is measured using the standard deviation of the most recent W-STD samples

$$\sigma_n = \sigma_{W-STD}(\omega_n) \tag{11}$$

A shorter window reacts quickly to abrupt changes but becomes sensitive to noise, whereas a longer window provides smoother behavior at the cost of responsiveness. A moderate window length 11 was chosen to balance these effects.

Then score is computed:

$$s_{n\,\omega} = clip\left(\frac{\sigma_n - min_\sigma}{max_\sigma - min_\sigma};\ 0, 2\right) \quad (12)$$

Here, the function $clip$ constrains the normalized value within the range of 0 to 2. A larger $s_{n\,\omega}$ indicates higher short-term instability. The upper bound of 2 allows the detection of fluctuations up to twice the level observed during typical AMR motion.

2. *Scoring CSI Amplitude Decrease*

Let max_{Amp} denote the maximum static-path amplitude observed so far and min_{Amp} denote the minimum amplitude observed so far. To ensure that these values represent the natural fluctuation range of the static component under LOS-like conditions, amplitude samples that are already identified as NLOS candidates (based on the combined score) are excluded from updating max_{Amp} and min_{Amp}. As a result, the upper and lower envelopes max_{Amp} and min_{Amp} are formed primarily from LOS or LOS-like samples.

Using these values, the attenuation score is defined as:

$$s_{n\,Amp} = clip\left(\frac{max_{Amp} - Amp_n}{max_{Amp} - min_{Amp}};\ 0, 2\right) \quad (13)$$

Scores above 1 correspond to drop in amplitude, indicating attenuation stronger than what is typically observed during LOS-like conditions.

3. *NLOS detection and Linear Interpolation*

The two scores are integrated into a combined NLOS confidence measure:

$$score_n = \omega_{weight} \cdot s_{n\,\omega} + Amp_{weight} \cdot s_{n\,Amp} \quad (14)$$

Here, the weighting parameters omega weight and amp weight were set to 0.4 and 0.6, respectively. Amplitude decrease was consistently observed as the dominant signature of NLOS-induced degradation, whereas angular fluctuations mainly captured rapid transitions around these intervals. Therefore, the combined score emphasizes amplitude while retaining angular variation as a supportive factor.

A point is labeled as NLOS when:

$$NLOS_n = \begin{cases} 1, \ if\ score_n \geq threshold \\ 0, \ otherwise \end{cases} \quad (15)$$

Because angular and amplitude variations do not perfectly distinguish LOS from NLOS, the threshold is not intended as a strict classifier but as a practical indicator of intervals where the AoA estimates are likely to become unreliable. In this study, the threshold was fixed at 1.2 which empirically highlighted segments where estimation errors tend to increase, even though the underlying propagation state may not be strictly NLOS. To avoid triggering interpolation due to momentary fluctuations or noise, correction is applied only when the threshold is exceeded continuously for at least 1.5 seconds. For each such interval, the AoA estimates are replaced with a linear interpolation between its endpoints, suppressing abrupt deviations while preserving continuity consistent with feasible AMR motion.

Algorithm: Filtering of AoA Estimates

Input:
Sequence of estimated angles $theta = \{\theta_1, \theta_2, \dots, \theta_N\}$
Received Dynamic CSI amplitude = $\{r_1, r_2, \dots, r_N\}$
Sampling interval Δt

Output:
Filtered angles $\theta_{filtered} = \{\theta_1, \theta_2, \dots, \theta_N\}$

#Params
W_STD // window length for std of angular velocity
THRESH // NLOS candidate threshold

Step 1: Scoring Angular Velocity
$\omega[n] \leftarrow (\theta[n] - \theta[n-1]) / \Delta t$
for each estimation n do
$\sigma_n \leftarrow$ std of ω over the last W_STD samples
maintain running min_σ, max_σ over σ_n
$s_{n\,\omega} \leftarrow$ clip($(\sigma_n - min_\sigma) / (max_\sigma - min_\sigma)$; $0, 2$))
end for

# Step 2: Scoring Dynamic CSI amplitude Decrease
for each estimation n do
maintain running min_{Amp}, max_{Amp}
$s_{n\,Amp} \leftarrow$ clip($(max_{Amp} - Amp_n)/(max_{Amp} - min_{Amp})$; $0, 2$))
end for

# Step 3: Detect NLOS and Linear Interpolate
for each estimation n do
$score_n \leftarrow \omega_{weight} \cdot s_{n\,\omega} + Amp_{weight} \cdot s_{n\,Amp}$
$NLOS_n \leftarrow$ if $score_n \geq$ THRESH else 0
for each NLOS segment [s,e] do
do linear comp between theta[s-1] and theta[e+1]
end for
end for

VI. Results and Discussion

Figure 7 shows the AoA estimation results after applying the proposed filtering method, and Figure 8 illustrates the linear interpolation applied to detected unreliable segments. Figure 7(a) summarizes the performance across the three trajectories ("N", "Z", and "V").

For Rx0 and Rx1, both in predominantly LOS regions, the median error improved modestly after filtering: from 0.20 to 0.17 rad and from 0.24 to 0.22 rad under EM-Shielding, and from 0.24 to 0.20 rad and 0.30 to 0.29 rad under No-EM-Shielding. These results show that the proposed method provides slight but consistent benefits even in LOS-dominant settings.

Rx2, positioned diagonally and experiencing frequent NLOS segments, exhibited much larger pre-filtering errors (0.64 rad under EM-Shielding and 0.51 rad under No-EM-Shielding). After filtering, both improved substantially: 0.64 to 0.47 rad (26.6% reduction) and 0.51 to 0.42 rad (17.1% reduction). This confirms that although shielding intensifies NLOS degradation by attenuating the direct path, the proposed method effectively mitigates such errors by correcting unstable intervals.

Aggregating all routes and receivers, the median AoA error improved from 0.35 rad to 0.30 rad (14.3%). Since the scoring-based detection is not a strict LOS/NLOS classifier, these gains arise from identifying periods where the MUSIC covariance matrix becomes unstable and smoothing them in accordance with feasible AMR motion.

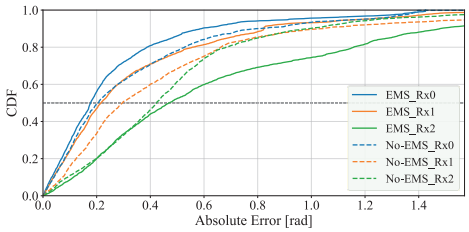

(a) CDF of AoA estimation results over all routes

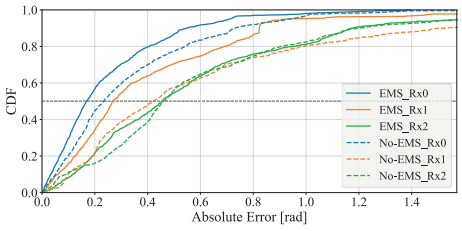

(b) CDF of AoA estimation results for "N" route

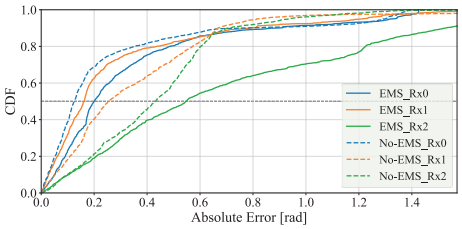

(c) CDF of AoA estimation results for "Z" route

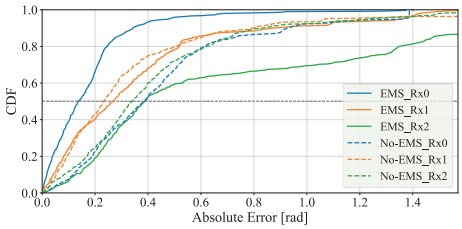

(d) CDF of AoA estimation results for "V" route

Fig. 7 CDF of AoA estimation results for each route after filtering

VII. Conclusion

This study examined the effect of electromagnetic shielding on dynamic AoA estimation using Wi-Fi CSI across three trajectories and three receivers with different LOS/NLOS characteristics. EM-Shielding improved accuracy in LOS-dominant regions (Rx0, Rx1) but degraded performance in NLOS-dominant regions (Rx2) due to stronger attenuation of the direct path.

To mitigate NLOS-induced degradation, we proposed a filtering method that combines angular fluctuation and static-path amplitude decrease to identify unreliable intervals, followed by linear interpolation. Rather than strictly classifying propagation states, the method targets periods where the MUSIC covariance structure becomes unstable. Across all trajectories, it improved the median AoA error by 14.3%, with larger gains in highly NLOS-dominant cases.

Although EM-Shielding was used as a controlled means to vary reflection strength, the results provide insight into practical device-free localization, where similar effects may arise with conductive clothing or objects. Future work includes parameter-sensitivity analysis, extension to multi-person scenarios, and evaluation for online implementations.

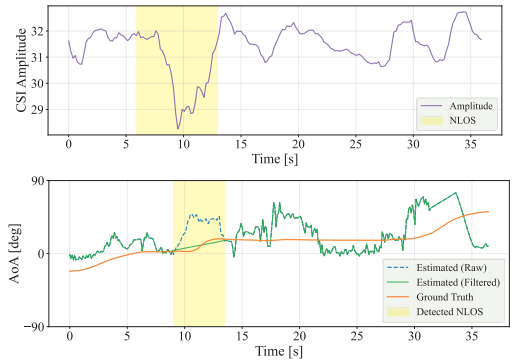

Fig.8 Linear interpolation process in filtering.

Acknowledgement

This work was supported by JSPS KAKENHI Grant Number 22K12016.

References

[1] M. Youssef, M. Mah, and A. Agrawala, “Challenges: Device-free Passive Localization for Wireless Environments,” Proc. ACM MobiCom ’07, pp. 222–229, Sept. 2007.

[2] M. Seifeldin, A. Saeed, A. E. Kosba, A. E-Keyi, and M. Youssef, “Nuzzer: A Large-Scale Device-Free Passive Localization System for Wireless Environments,” IEEE Trans. on Mobile Computing, vol. 12, no. 7, pp. 1321–1334. July 2013.

[3] R. Steele, Amanda Lo, C. Secombe, and Y. Kuen Wong, “Elderly persons’ perception and acceptance of using wireless sensor networks to assist healthcare,” International Journal of Medical Informatics, vol. 78, no. 12, pp. 788–801. Aug. 2009.

[4] P. Bahl and V. N. Padmanabhan, “RADAR: An in-building RF-based user location and tracking system,” Proc. IEEE INFOCOM Mar. 2000.

[5] M. Kotaru, K. Joshi, D. Bharadia, and S. Katti, “SpotFi: Decimeter level localization using WiFi,” ACM SIGCOMM Computer Communication Review, vol. 45, no. 4, pp. 269–282. Aug. 2015.

[6] Z. Yang, Z. Zhou, and Y. Liu, “From RSSI to CSI: Indoor Localization via Channel Response,” ACM Computing Surveys. vol. 46, no. 2, Article no:25, pp. 1–25, Dec. 2013.

[7] M. Goel, C. Zhao, R. Vinisha, and S. N. Patel, “Tongue-in-Cheek: Using Wireless Signals to Enable Non-Intrusive and Flexible Facial Gestures Detection,” Proc. ACM CHI ‘15, pp. 255–258. Apr. 2015.

[8] Q. Pu, S. Gupta, S. Gollakota, and S. Patel, “Whole-home Gesture Recognition Using Wireless Signals,” Proc. ACM MobiCom ‘13, pp. 27–38. Sept. 2013.

[9] J. Xiong and K. Jamieson, “ArrayTrack: A fine-grained indoor location system,” Proc. of the 10th USENIX conference on Networked Systems Design and Implementation (nsdi '13), pp. 71–84, Apr. 2013.

[10] Y. Ma, G. Zhou, and S. Wang, “Dynamic-MUSIC: Accurate device-free indoor localization,” Proc. ACM Int. Joint Conf. Pervasive and Ubiquitous Computing (UbiComp ‘16), pp. 196–207. Sept. 2016.

[11] H. A-Nasser, R. Samir, I. Sabek, and M. Youssef, “MonoPHY: Mono-stream-based device-free WLAN localization via physical layer information,” Proc. IEEE WCNC 2023, Apr. 2013.

[12] K. Ohara, Y. Kishino, A. Fujino, and H. Sawada, “A study on CFO removal for device-free passive localization using AoA of Wi-Fi signals,” Proc. IEICE General Conf., vol. 1, no. B-15-13, Mar. 2025. (in Japanese)

[13] K. Qian, C. Wu, Z. Yang, Y. Liu, and K. Jamieson, “Widar2.0: Passive human tracking with a single Wi-Fi link,” Proc. 16th ACM Int. Conf. Mobile Systems, Applications, and Services (MobiSys ‘18), pp. 350–361. Jun. 2018.

[14] D. Wu, D. Zhang, C. Xu, H. Wang, and Z. Yu, “WiTraj: Robust indoor motion tracking with WiFi signals,” IEEE Trans. Mobile Comput., vol. 22, no. 5, pp. 3062–3078, Dec. 2021.